The complex interface chemistry of thin-film silicon/zinc oxide solar cell structures

Gerlach, D.; Wimmer, M.; Wilks, R. G.; Félix, R.; Kronast, F.; Ruske, F.; Bär, M.

Published in:
Physical Chemistry Chemical Physics

DOI:
10.1039/c4cp03364g

Publication date:
2014

PCCP

PAPER

View Article Online
View Journal | View Issue

Cite this: *Phys. Chem. Chem. Phys.*, 2014, **16**, 26266

The complex interface chemistry of thin-film silicon/zinc oxide solar cell structures

D. Gerlach,*[ab] M. Wimmer,[a] R. G. Wilks,[a] R. Félix,[a] F. Kronast,[c] F. Ruske[a] and M. Bär*[ad]

Received 29th July 2014,
Accepted 27th October 2014

DOI: 10.1039/c4cp03364g

www.rsc.org/pccp

The interface between solid-phase crystallized phosphorous-doped polycrystalline silicon (poly-Si(n^+)) and aluminum-doped zinc oxide (ZnO:Al) was investigated using spatially resolved photoelectron emission microscopy. We find the accumulation of aluminum in the proximity of the interface. Based on a detailed photoemission line analysis, we also suggest the formation of an interface species. Silicon suboxide and/or dehydrated hemimorphite have been identified as likely candidates. For each scenario a detailed chemical reaction pathway is suggested. The chemical instability of the poly-Si(n^+)/ZnO:Al interface is explained by the fact that SiO_2 is more stable than ZnO and/or that H_2 is released from the initially deposited a-Si:H during the crystallization process. As a result, Zn (a deep acceptor in silicon) is "liberated" close to the silicon/zinc oxide interface presenting the inherent risk of forming deep defects in the silicon absorber. These could act as recombination centers and thus limit the performance of silicon/zinc oxide based solar cells. Based on this insight some recommendations with respect to solar cell design, material selection, and process parameters are given for further knowledge-based thin-film silicon device optimization.

Introduction

Decreased material consumption and the possibility of low-cost and energy efficient production with an abundant and non-toxic material are the main attractions of silicon based thin-film solar cells. While cell efficiency lags behind that of wafer-based silicon solar cells, multiple routes to produce high-quality thin-film silicon are in development to close the performance gap.

One fabrication route is the direct deposition of hydrogenated amorphous silicon (a-Si:H) thin films and the use of solid-phase crystallization (SPC, at approx. 600–650 °C) to convert a-Si:H to polycrystalline silicon (poly-Si) that is resistant to light-degradation.[1] While poly-Si based solar cell mini modules have achieved reasonable efficiencies,[2] the next challenge is the implementation of a transparent conductive oxide (TCO) front contact, such as aluminum-doped zinc oxide (ZnO:Al), for the ease of electrical contacting and implementation of light trapping schemes.[3]

During solar cell fabrication the a-Si:H and/or poly-Si/ZnO:Al layer stack undergoes multiple post-deposition annealing steps for SPC and defect passivation (by, *e.g.*, rapid thermal annealing – RTA – at approx. 950 °C) that are suspected to impact the chemical and electronic silicon/zinc oxide interface structure limiting the performance of resulting thin-film silicon solar cells. The silicon/zinc oxide interface was investigated previously with soft X-ray emission spectroscopy (XES),[4] hard X-ray photoelectron spectroscopy (HAXPES),[5,6] and X-ray absorption spectroscopy.[7] These studies report that the chemical structure of the silicon/zinc oxide interface changes significantly after the thermal treatments.[4–7] Furthermore, indications have been found that Zn and Al atoms – from the aluminum doped zinc oxide – accumulate at the silicon/ZnO:Al interface and/or diffuse into the Si cover layer upon SPC.[4–6] Recently, liquid-phase crystallization of a-Si:H layers by laser or e-beam has led to poly-Si absorber layers with superior electrical quality.[8,9] Despite the short treatment times for liquid-phase crystallization, it is expected that the harsher conditions and the silicon liquidification and crystallization will affect adjacent interfaces and hence enhances the need to study interface reactions between silicon and oxide materials, which are already used as passivation (*e.g.*, SiO_2) or contacting (*e.g.*, TCOs) layers that could be employed in next-generation thin-film silicon based devices.

Employing a photoemission electron microscope (PEEM), we use spatially resolved photoemission in combination with a deliberate sample design to gain a deeper insight into the

[a] *Renewable Energies, Helmholtz-Zentrum Berlin für Materialien und Energie, Hahn-Meitner-Platz 1, D-14109 Berlin, Germany. E-mail: marcus.baer@helmholtz-berlin.de*
[b] *MANA/Nano-Electronics Materials Unit, National Institute for Materials Science (NIMS), 1-1 Namiki, Tsukuba, Ibaraki 305-0044, Japan. E-mail: GERLACH.Dominic@nims.co.jp*
[c] *Department for Magnetisation Dynamics, Helmholtz-Zentrum Berlin für Materialien und Energie GmbH, Albert-Einstein-Str. 15, D-12489 Berlin, Germany*
[d] *Institut für Physik und Chemie, Brandenburgische Technische Universität Cottbus-Senftenberg, Platz der Deutschen Einheit 1, D-03046 Cottbus, Germany*

chemical structure of the silicon/(aluminum-doped) zinc oxide interface after SPC. In this paper, we specifically focus on the still open questions of interface species identification and the Zn and Al (re)distribution in the proximity of this interface as the basis for a detailed model for the complex interface chemistry. As a result the limiting factors of the silicon/zinc oxide interface in a solar cell device are identified and alternative pathways with respect to solar cell design, material selection, and process parameters – circumventing these obstacles – recommended.

Experimental

Using plasma-enhanced chemical vapor deposition (PECVD), approximately 5 nm phosphorous-doped hydrogenated amorphous silicon (a-Si:H(P)) was deposited on 650 nm thick magnetron-sputtered aluminum-doped zinc oxide films on Corning Eagle® glass substrates.[10] Subsequently, the deposited a-Si:H(P)/ZnO:Al structure was subject to SPC, *i.e.*, annealing for 24 hours at 650 °C under N_2 atmosphere. For standard thicknesses, this results in a poly-Si(n^+)/ZnO:Al layer stack. Right before introducing the samples into the ultra-high vacuum PEEM analysis system (base pressure 5×10^{-10} mbar) for measurements, the thin poly-Si layer was partly mechanically removed, followed by a HF-treatment (10 s in 0.5% HF) to remove the (natively formed) surface oxide.

The X-ray photoelectron emission microscopy (X-PEEM) measurements were performed at the SPEEM endstation – a modified Elmitec PEEM II system[11] – permanently installed at the UE49-PGMa APPLE-II undulator microfocus beamline of the BESSY II synchrotron radiation facility. Horizontally polarized X-rays with the polarization vector directed towards the PEEM entrance were used at grazing incidence sample orientation. The PEEM images have been recorded with an accelerator voltage between sample and objective lens of 10 keV and a field of view (FOV) of 10 μm. The images have been normalized to (*i.e.*, divided by) a brightfield image recorded directly before the actual measurements to account for detector characteristics.

Element specificity is achieved by tuning the excitation energy and analyzer energy to focus on a particular characteristic photoemission line. The excitation energy was selected such that the kinetic energy of each photoemission line being studied was roughly the same (*ca.* 200 eV), and so effects such as detector transmission variations and differing electron inelastic mean free paths can be neglected for data evaluation. Changing the excitation energy, rather than the kinetic energy, additionally allows one to select particular photoemission lines without refocusing the microscope. The presented data is based on X-PEEM difference images calculated by subtracting an image recorded at the off-resonance photoemission (*i.e.*, the background signal recorded at *ca.* 5 eV lower binding energy than the photoemission line of interest) from the image recorded at the on-resonance photoemission energy.

Results

A spatially integrating XPS survey spectrum, measured at 250 eV excitation energy, reveals contributions from Si, Zn, Al, O, and C. Fig. 1 shows this data, concentrating on the spectral region containing the Si 2p, Zn 3p and Al 2p photoemission lines. The two Si 2p photoemission peaks at E_{Si1} = (102.8 ± 0.3) eV and E_{Si2} = (99.6 ± 0.3) eV can be ascribed to Si–O_2 bonds and Si–Si bonds, respectively.[12] Note that the Si 2p doublet separation of approximately 0.6 eV could not be resolved with the instrument settings used, however the Zn 3p doublet (2.7 eV separation) is resolved.[12] The energetic position of the Zn $3p_{3/2}$ line at E_{Zn} = (89.3 ± 0.3) eV is in agreement with Zn in ZnO.[12] The Al 2p binding energy (doublet separation of approximately 0.4 eV) of (75.0 ± 0.3) eV is indicative for aluminum in ZnO:Al.[12,13]

Fig. 2(a) shows a secondary electron emission image with a field of view (FOV) of 10 μm. The FOV was chosen such that both an area in which the poly-Si(n^+) was mechanically removed from the ZnO:Al (area (A) in Fig. 2c) and an area in which the thin poly-Si(n^+) covers the ZnO:Al (area (B) in Fig. 2c) could be probed. Due to the lower work function of ZnO:Al (3.5 eV), compared to that of Si (4.5–4.9 eV),[15,16] the exposed ZnO:Al on the upper part of the image appears much brighter. Fig. 2(b) shows the same FOV in an energy-filtered X-PEEM image: while exciting the sample at $h\nu$ = 305 eV, electrons were collected at 200.6 eV kinetic energy (E_{kin}) making the image sensitive to the Si 2p photoemission signal. More specifically, this image represents the spatial distribution of the Si 2p photoemission signature of oxidized silicon (*i.e.*, the energy of probed electrons corresponds to E_{Si1}). Fig. 2(c) is retrieved in the same fashion but with an excitation energy of $h\nu$ = 216 eV, which results in a Zn 3d (binding energy approx. 10 eV) sensitive X-PEEM image.[12] Maintaining the same kinetic energy results in the same inelastic mean free path of approximately 0.8 nm [IMFP calculated for a silicon cover layer using the QUASES-IMFP-TPP2M[14] code based on TPP2M formula in ref. 17] and thus information depth for the Si 2p and Zn 3d photoelectrons.

The Si 2p (Fig. 2b) and Zn 3d (Fig. 2c) photoemission intensity maps appear to be inverses, which confirms that the upper part of the FOV is the exposed, and the lower part of the FOV the poly-Si(n^+) covered, ZnO:Al, divided by an abrupt edge. Except for the upper part of the FOV, a mostly uniform Si cover

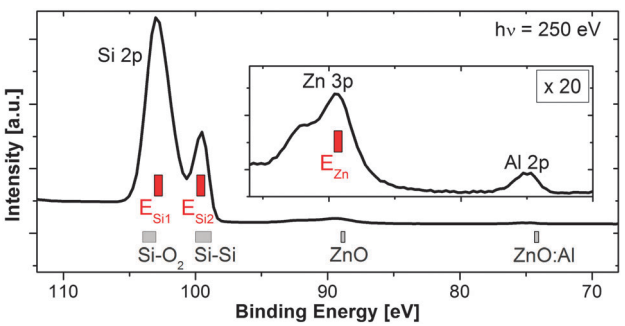

Fig. 1 Spatially integrating photoemission spectrum of the 5 nm poly-Si(n^+)/ZnO:Al sample taken at 250 eV excitation energy. The insert magnifies the Zn 3p and Al 2p peaks on the same energy scale. Specific energy positions E_{Si1}, E_{Si2} and E_{Zn} are indicated and are referred to in the text and the following figures. Literature values for Si 2p, Zn 3p, and Al 2p (indicating Si–O_2 and Si–Si bonds as well as ZnO and ZnO:Al, respectively) are presented as gray bars for comparison.[12,13]

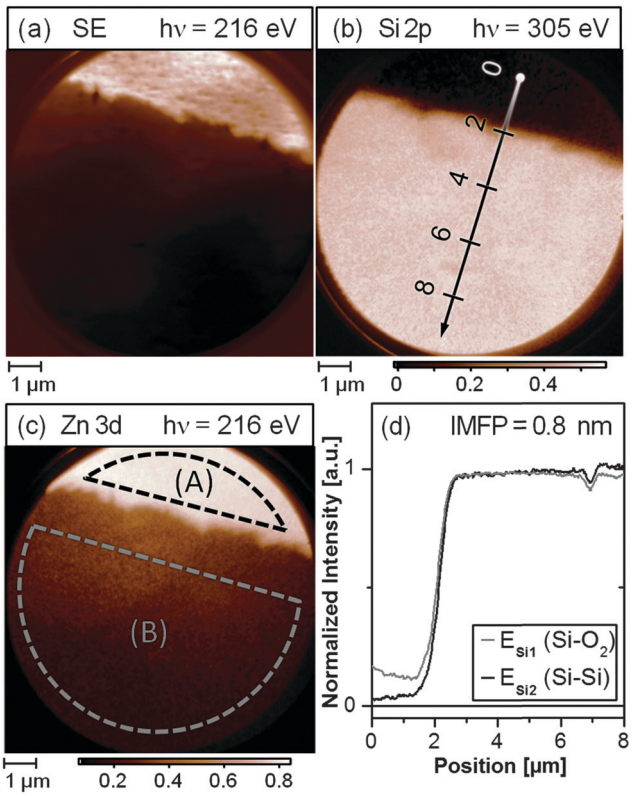

Fig. 2 Secondary electron (SE) image measured at 216 eV (a) and X-PEEM images at 305 eV for Si 2p (b) and at 216 eV excitation energy for Zn 3d (c) of the 5 nm poly-Si(n^+)/ZnO:Al sample. The excitation energy was chosen such that it results in the same inelastic mean free paths (IMFP = 0.8 nm[14]), and hence information depth, for the data depicted in (b) and (c). The photoemission intensity is color coded according to the scales shown at the bottom. A Si 2p line scan (d) illustrates the intensity evolution along the axis shown in (b) for energies E_{Si1} and E_{Si2} (see Fig. 1). Here the intensity was normalized to the 4 µm position.

layer can be observed in the Si 2p X-PEEM image. Darker specks are most likely due to contamination on the surface or other topographical features, as they do not show up as bright spots in the Zn 3d X-PEEM image. Fig. 2(d) shows computed photoemission intensity line scans of the Si 2p (E_{Si1}: Si–O_2) X-PEEM image (Fig. 2b) and of a Si 2p (E_{Si2}: Si–Si) X-PEEM image (not shown) along the arrow indicated in Fig. 2(b) using an integration width of 2 µm. To directly compare the derived scans, the intensity is normalized to the corresponding intensity values at the 4 µm position. The dip at the 7 µm position corresponds to a dark speck in Fig. 2(b), most likely due to surface contamination as discussed above. The Si–O_2/Si–Si ratio below 2 µm (*i.e.*, in the exposed region) is much higher than in the covered area, suggesting that an oxidized silicon phase is present on the surface of the exposed ZnO:Al layer. Note that a diffusion of silicon into the zinc oxide (and the subsequent formation of Si–O_2 bonds), as predicted in ref. 18, would also explain this finding.

For a more detailed analysis, area-integrated detail spectra of the exposed region (A) and the covered region (B) [as indicated in Fig. 2(c)] have been computed and are shown in Fig. 3. While spectrum (B) is similar to the dispersive plane spectrum of Fig. 1, spectrum (A) shows enhanced Zn 3p and Al 2p photoemission peaks as expected for a spectrum of the exposed ZnO:Al area. More surprisingly, the Si 2p photoemission line consists primarily of a single peak with a chemically-shifted binding energy in-between E_{Si1}(Si–O_2) and E_{Si2}(Si–Si) of spectrum (B). [Note that this may result in an underestimation of the oxidized silicon signal intensity in the line scan shown in Fig. 2(d).] The Zn 3p and Al 2p detail spectra of area (A) and (B) are compared in the inset of Fig. 3 after a 6th order polynomial background correction and normalization to the peak intensities of the Zn 3p line. The relative Al 2p intensity in area (B) is much higher. When considering the corresponding photoemission cross sections,[19] the different Al 2p/Zn 3p intensity ratios translate into Al/Zn ratios of (1.6 ± 0.8)% for area (A) and (4.1 ± 2.0)% for area (B). Note that the stated experimental uncertainty reflects the low signal-to-noise ratio and difficulties to reliably account for the spectral background. The Al/Zn ratio in area (A) agrees very well with the expected Al/Zn composition considering the 1 wt% Al content in the ZnO:Al sputter target that results in ZnO:Al layers with an Al/Zn ratio of 1.6%. The fact that we find an enhanced Al content in the covered area (B) might be indicative for a diffusion and/or accumulation of Al into the silicon cover layer and/or at the silicon/zinc oxide interface, confirming our earlier results of an SPC-induced Al redistribution.[6]

In order to identify the potentially formed interface species, the Si 2p and Zn 3p peaks have been further analyzed (see Fig. 4). After subtraction of a linear background, the Zn 3p spectra of area (A) and (B) were simultaneously fitted with two coupled Voigt profiles of the same Gaussian and Lorentzian

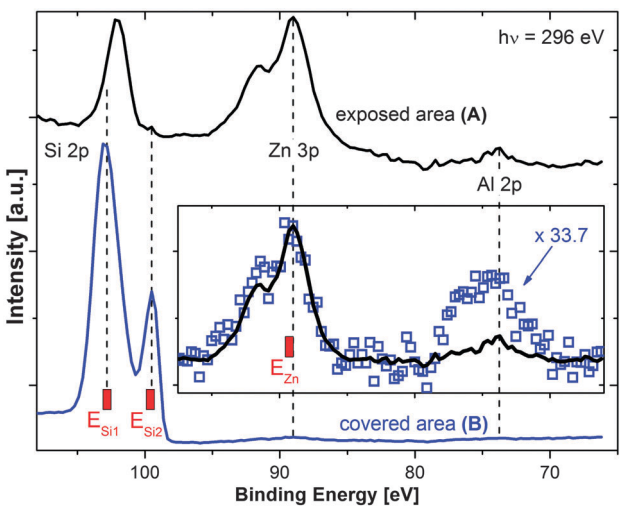

Fig. 3 Local XPS spectra of the exposed area (A) and the covered area (B) defined in the Zn 3d X-PEEM image of Fig. 2(c). The inset shows background corrected spectra (normalized to the maximum of the Zn 3p photoemission line) of these areas to compare the relative Al 2p intensity. The scatter plot represents the spectrum of area (B) and the respective normalization factor is stated. The binding energies E_{Si1}, E_{Si2}, and E_{Zn} as defined in Fig. 1 and vertical dashed lines (as a guide to the eye) are indicated to compare peak positions.

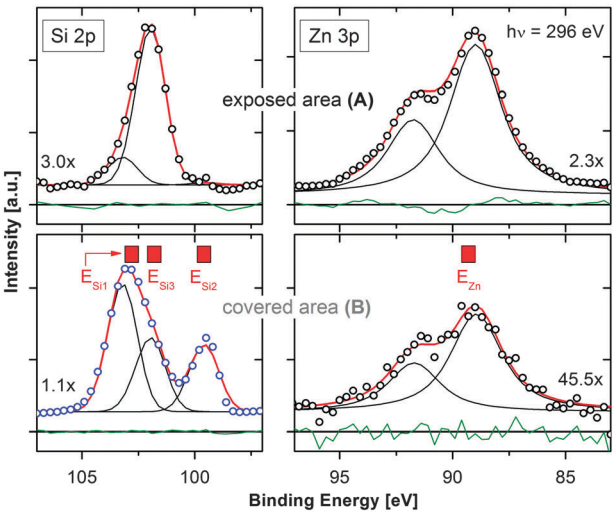

Fig. 4 Fits of the local Si 2p (left panels) and Zn 3p (right panels) XPS spectra of the exposed area (A) (top panels) and the covered area (B) (bottom panels). Open symbols indicate the data, solid lines the fit (red), individual fit components (black), and the residua (green). The binding energies E_{Si1}, E_{Si2}, and E_{Zn} as defined in Fig. 1 are indicated to compare peak positions. Note that for the Si 2p fit, the individual Si $2p_{3/2}$ and Si $2p_{1/2}$ contributions have been considered, but only the doublet is depicted. Intensity scaling factors and residua are also indicated.

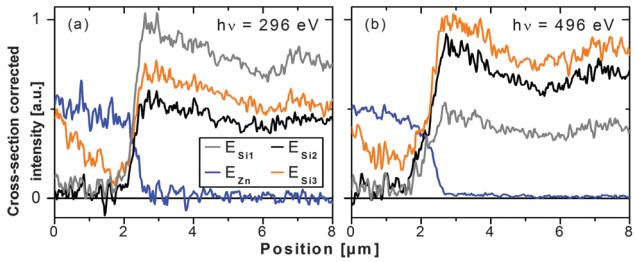

Fig. 5 X-PEEM intensity line scans recorded (a) at 296 eV (*i.e.*, with an IMFP of 0.8 nm[14]) and (b) at 496 eV (*i.e.*, with an IMFP of 1.2 nm[14]) along the arrow shown in Fig. 2(b). The photo ionization cross section (from ref. 20) corrected line scans are shown for binding energies E_{Si1}(Si–O_2), E_{Si2}(Si–Si), E_{Si3}, and E_{Zn}(Zn–O).

width, an intensity ratio according to the $2j + 1$ multiplicity (*i.e.*, 2 : 1), and a fixed doublet separation of 2.7 eV.[12] The position of the Zn $3p_{3/2}$ is (88.9 ± 0.3) eV and (88.8 ± 0.3) eV in the exposed (A) and covered (B) area, respectively, both of which are in agreement with Zn in a ZnO environment (as discussed above).[12] After subtraction of a linear background, the Si 2p detail spectra of area (A) and (B) were simultaneously fitted with three coupled Voigt profile pairs having the same Lorentzian and Gaussian widths. The intensity ratio of the profile doublet was again set according to the $2j + 1$ multiplicity (*i.e.*, 2 : 1) and the spin–orbit doublet separation was set to 0.6 eV.[12] As above, the Si $2p_{3/2}$ contribution at (99.4 ± 0.3) eV can be attributed to Si–Si bonds while the contribution at (103.0 ± 0.3) eV represents Si–O_2 bonds.[12] Furthermore, an additional peak between the Si 2p Si–Si and Si–O_2 contributions can be identified in both the spectra of the exposed (A) and covered (B) area. Note that the Si 2p spectrum of area (A) is dominated by this intermediate line at E_{Si3} = (101.8 ± 0.3) eV and that only a minor Si–Si contribution is observed in this case.

To test whether the Si $2p_{3/2}$ line at E_{Si3} represents an interface species, we consult the cross-section-corrected photoemission intensity line scans along the arrow indicated in Fig. 2(b).[20] The intensities are shown for lines at E_{Si1}(Si–O_2), E_{Si2}(Si–Si), E_{Si3}, and E_{Zn}(Zn–O) recorded for two excitation energies $h\nu$ = 296 eV (IMFP = 0.8 nm[14]) and $h\nu$ = 496 eV (IMFP = 1.2 nm[14]) in Fig. 5(a) and (b), respectively. When comparing the line scans of the more surface-sensitive data in Fig. 5(a) with the more bulk-sensitive data in Fig. 5(b), we find a significant increase of the E_{Si2}/E_{Si1} [*i.e.*, (Si–Si)/(Si–O_2)] ratio and an almost unchanged E_{Si2}(Si–Si)/E_{Si3} in the covered area (*i.e.*, 2–8 μm). This indicates that the Si–O_2 covers the Si–Si and the "E_{Si3} species," and that the latter species is primarily present on top and/or in the surface region of the ZnO:Al layer. The Si $2p_{3/2}$ binding energy of the "E_{Si3} species" is at higher energies [ΔE = (+2.4 ± 0.4) eV] than the Si $2p_{3/2}$ Si–Si contribution. Previously, this was attributed to a "Si^{3+}" oxidization state (ΔE = +2.48 eV[21]) interpreted as being indicative for a silicon suboxide: Si_2O_3. However, in ref. 22 the Si $2p_{3/2}$ photoemission of hemimorphite ($Zn_4Si_2O_7(OH)_2{\cdot}H_2O$) was found at 101.76 eV, which would – within the experimental uncertainty – also agree very well with E_{Si3}. Note that the Si $2p_{3/2}$ of Zn_2SiO_4 – a species suggested to be formed at the interface of the inverse layer stack, in particular when ZnO films are sputtered on Si-wafers[23] and when these stacks are thermally treated at temperatures >approximately 800 °C[24,25] – is reported to be at (102.4–102.6 eV[23,26]) and thus does not agree with E_{Si3}, even taking the conservatively estimated experimental uncertainty into account.

Hence, there are two equivalent scenarios explaining the presence of the "E_{Si3} species." Scenario (I) is based on the attribution of E_{Si3} to a silicon suboxide formed at the poly-Si(n^+)/ZnO:Al interface, *e.g.*, at the expense of Zn–O bonds as proposed in ref. 27 and experimentally shown in ref. 5.

$$y\mathrm{ZnO} + x\mathrm{Si} \rightarrow \mathrm{Zn} + \mathrm{Si}_x\mathrm{O}_y \qquad (1)$$

This is in-line with the suggestion by Amekura *et al.*[28] that Si-implanted into a ZnO matrix will form a silicon (sub)oxide upon annealing. The chemical driving force for this process is caused by the fact that silicon oxide is more stable than zinc oxide.[27] Note that an incomplete removal of the silicon cover layer from the underlying zinc oxide and the subsequent partial oxidation of the silicon residue could also be an explanation for the observed presence of a silicon suboxide in the uncovered area. In the (more complex) scenario (II), E_{Si3} is ascribed to – due to the thermal SPC treatment – slightly modified, *i.e.*, dehydrated hemimorphite, $Zn_4Si_2O_7(OH)_2$. Hydrated zinc silicate hydroxide, *i.e.*, hemimorphite ($Zn_4Si_2O_7(OH)_2{\cdot}H_2O$) loses its molecule water at temperatures between 393 °C and 657 °C.[29] Note that the impact of the dehydration of hemimorphite on the respective Si $2p_{3/2}$ binding energy can be expected to be negligible. The formation of this dehydrated hemimorphite at the interface between silicon and zinc oxide

can be explained by a multistep process that starts with the dehydrogenation of the a-Si:H in the initial SPC stages according to eqn (2).[30] This process generally starts at temperatures of 350–400 °C.[30,31]

$$2\text{a-Si:H} \rightarrow 2\text{poly-Si} + H_2 \quad (2)$$

Subsequently, the hydrogen released close to the silicon/zinc oxide interface could result in a reduction of zinc oxide, forming metallic zinc (see eqn (3)) as is proposed to take place for bulk ZnO for temperatures >600 °C in ref. 32.

$$ZnO + H_2 \leftrightarrow Zn + H_2O \quad (3)$$

The formed (gaseous) water could then result in the oxidation of the interfacial silicon as described in eqn (4a). Alternatively, the silicon could also be oxidized by residual oxygen in the SPC tube furnace following the process described by eqn (4b). Both the ''wet-oxidation'' (4a) and the ''dry-oxidation'' (4b) of silicon start at temperatures similar to the 650 °C used for the SPC treatment.[33,34]

$$Si + 2H_2O \rightarrow SiO_2 + 2H_2 \quad (4a)$$

$$Si + O_2 \rightarrow SiO_2 \quad (4b)$$

Under these circumstances ZnO, SiO_2, and H_2O are present at the silicon/zinc oxide interface, and thus it can be speculated that (dehydrated) hemimorphite is hydrothermally synthesized as proposed in ref. 35.

$$4ZnO + 2SiO_2 + H_2O \rightarrow Zn_4Si_2O_7(OH)_2 \quad (5)$$

For the availability of water and silicon oxide as educts for reaction (5) it is not necessarily required to follow routes (3) and (4); they could also be provided *via* the reaction of the liberated hydrogen with residual oxygen in the SPC tube furnace and through the process described in scenario (I), respectively. Based on the available data no scenario can be favored and thus a silicon suboxide (→ scenario I) and/or a (dehydrated) hemimorphite (→ scenario II) could be formed as an interface species. Correspondingly, the ''decomposition'' of the (aluminum-doped) zinc oxide may take place according to scenario (I) (eqn (1)) and/or (II) (eqn (3) and (5)). The resulting ''liberation'' of zinc (and aluminum) is in agreement with the observed SPC-induced elemental redistribution of Zn and Al in the proximity of the poly-Si(n^+)/ZnO:Al interface.[5,6] Based on the discussion in conjunction with the inset of Fig. 3 (above) and ref. 6, it was found that this redistribution is more pronounced for Al than for Zn, *i.e.*, more Al (than Zn) accumulates at the poly-Si(n^+)/ZnO:Al *interface* and/or Al is located closer to the poly-Si(n^+)/ZnO:Al sample *surface*. Considering that the accumulation of aluminum in silicon oxide is preferred over that in silicon,[36] the latter explanation would be in agreement with both scenario (I) and the formation of a silicon oxide ''reaction front'' located between the poly-Si top layer and the hemimorphite interface species (scenario II).

Correspondingly, the reported formation of Zn_2SiO_4 upon annealing at higher temperatures (≥950 °C) as used for RTP,[7] can be explained by the solid-state reaction of zinc oxide and silicon (sub)oxide (forming Zn_2SiO_4) as reported in ref. 37 for temperatures between 800 °C and 1000 °C and/or the dehydroxylation of $Zn_4Si_2O_7(OH)_2$, which starts at temperatures >700 °C.[38] Similarly, the RTP-induced formation of Al_xO_y at the poly-Si(n^+)/ZnO:Al interface as suggested by Becker *et al.*,[7] is in accordance with the formation of aluminum oxide at the expense of the reduction of SiO_2, which is reported to take place in the Al–SiO_2 material system for temperatures >700 °C.[39] Based on secondary ion mass spectroscopy depth profiles, it was also reported that after RTP a pronounced zinc diffusion into the poly-Si takes place, while aluminum mainly stays (as Al_xO_y) in the proximity of the poly-Si(n^+)/ZnO:Al interface.[7] At first, this seems to contradict our finding that Al shows the higher degree of SPC-induced interfacial redistribution. The fact that no significant diffusion of zinc in silicon below SPC temperature < approximately 700 °C < RTP temperature is documented[40] and that the aluminum is – according to the above suggested oxide formation mechanism – practically confined to the poly-Si(n^+)/ZnO:Al interface, however, explains both experimental observations.

Although one cannot exactly pin down the interface chemistry taking place for thin-film silicon/(aluminum-doped) zinc oxide solar cell structures upon post-deposition thermal treatments, it is possible to identify the limiting driving forces. The chemical interaction at, and thus instability of, the poly-Si(n^+)/ZnO:Al interface is caused by the fact that SiO_2 is more stable than ZnO (→ scenario (I)) and/or that H_2 is released from the initially deposited a-Si:H by SPC induced dehydrogenation (→ scenario (II)). In consequence, to improve the stability of thin-film silicon based interfaces it is recommended to (i) employ an alternative transparent conductive oxide (TCO) which is stable in contact to silicon also at high temperatures, (ii) directly deposit poly-Si or reduce the H_2 content in the a-Si layer, and/or (iii) introduce a chemically inert barrier layer between the thin-film silicon and the ZnO:Al TCO.

With respect to recommendation (i), and solely based on the thermodynamic stability in contact with silicon, *e.g.*, ZrO_2 would be a suitable candidate to replace ZnO[27] – if one could manage to enhance its conductivity. Directly depositing poly-Si [→ (ii)] is definitely a viable route to minimize hydrogen content in the silicon thin film but usually does not lead to the same material quality as yielded by SPC of a-Si:H. If scenario (II) would be the dominating one, then one could add a low-temperature annealing step at around 400 °C (for dehydrogenation) before going to 600–650 °C for SPC. This would be a way to avoid ZnO decomposition (according to eqn (3)), as it will only take place in the presence of H_2, but not at temperatures below 600 °C.[32] Using, *e.g.*, a Si_xN_y barrier layer [→ (iii)] the diffusion of zinc into the silicon thin film can be prevented.[7] This not only improves the stability of the interface but also inhibits the Zn-impurity induced formation of deep energy levels that can act as recombination centers.[41] Avoiding ZnO decomposition and thus preventing zinc from being formed close to the interface might, hence, also be the key to improve the performance of thin-film solar cells based on silicon/zinc oxide structures.

Conclusion

In summary, we used spatially resolved X-PEEM to study the chemical structure of the silicon/(aluminum-doped) zinc oxide interface. We find indications for Al diffusing into the silicon and/or its accumulation in the proximity of the interface. Furthermore, the presence of a new silicon species at the poly-Si(n^+)/ZnO:Al interface was revealed. Silicon suboxide (Si_2O_3) or dehydrated hemimorphite ($Zn_4Si_2O_7(OH)_2$) are plausible candidates. For each scenario chemical reaction pathways are suggested and discussed. Most detrimental for the solar cell performance is most likely the finding that Zn (which can form deep recombination centers in silicon) is ''liberated'' close to the interface in both cases. The fact that SiO_2 is more stable than ZnO and/or that H_2 is released from the initially deposited a-Si:H have been identified as the main factors for the chemical instability of the poly-Si(n^+)/ZnO:Al interface. Based on this insight some recommendations with respect to solar cell design, material selection, and process parameters are given for further knowledge-based device optimization.

Acknowledgements

We thank J. Hüpkes from Forschungszentrum Jülich for providing ZnO:Al substrates. D.G., R.G.W., R.F., and M.B. acknowledge financial support by the Helmholtz-Association (VH-NG-423). D.G. additionally thanks the Japan Society for the Promotion of Science (PE 13070).

Notes and references

1 M. A. Green, *Appl. Phys. A: Mater. Sci. Process.*, 2009, **96**, 153.
2 M. Keevers, T. Young, U. Schubert, M.A. Green, presented at 22nd EU PVSEC, Milan, September, 2007.
3 O. Kluth, B. Rech, L. Houben, S. Wieder, G. Schöpe, C. Beneking, H. Wagner, A. Löffl and H. W. Schock, *Thin Solid Films*, 1999, **351**, 247.
4 M. Bär, M. Wimmer, R. G. Wilks, M. Roczen, D. Gerlach, F. Ruske, K. Lips, B. Rech, L. Weinhardt, M. Blum, S. Pookpanratana, S. Krause, Y. Zhang, C. Heske, W. Yang and J. D. Denlinger, *Appl. Phys. Lett.*, 2010, **97**, 072105.
5 M. Wimmer, M. Bär, D. Gerlach, R. G. Wilks, S. Scherf, C. Lupulescu, F. Ruske, R. Félix, J. Hüpkes, G. Gavrila, M. Gorgoi, K. Lips, W. Eberhardt and B. Rech, *Appl. Phys. Lett.*, 2011, **99**, 152104.
6 M. Wimmer, D. Gerlach, R. G. Wilks, S. Scherf, R. Félix, C. Lupulescu, F. Ruske, G. Schondelmaier, K. Lips, J. Hüpkes, M. Gorgoi, W. Eberhardt, B. Rech and M. Bär, *J. Electron Spectrosc. Relat. Phenom.*, 2013, **190**(part B), 309.
7 C. Becker, M. Pagels, C. Zachäus, B. Pollakowski, B. Beckhoff, B. Kanngießer and B. Rech, *J. Appl. Phys.*, 2013, **113**, 044519.
8 J. Dore, D. Ong, S. Varlamov, R. Egan and M. A. Green, *IEEE J. Photovolt.*, 2014, **4**, 33.
9 D. Amkreutz, J. Haschke, T. Häring, F. Ruske and B. Rech, *Sol. Energy Mater. Sol. Cells*, 2014, **123**, 13.
10 M. Berginski, J. Hüpkes, M. Schulte, G. Schöpe, H. Stiebig, B. Rech and M. Wuttig, *J. Appl. Phys.*, 2007, **101**, 074903.
11 F. Kronast, J. Schlichting, F. Radu, S. K. Mishra, T. Noll and H. A. Dürr, *Surf. Interface Anal.*, 2010, **42**, 1532.
12 National Institute of Standards and Technology, NIST X-ray Photoelectron Spectroscopy (XPS) Database, http://srdata.nist.gov/xps/Default.aspx, accessed April 2014.
13 M. Chen, X. Wang, Y. H. Yu, Z. L. Pei, X. D. Bai, C. Sun, R. F. Huang and L. S. Wen, *Appl. Surf. Sci.*, 2000, **158**, 134.
14 S. Tougaard, QUASES-IMFP-TPP2M, http://www.quases.com/products/quases-imfp-tpp2m/, accessed July 2012.
15 A. Klein, C. Körber, A. Wachau, F. Säuberlich, Y. Gassenbauer, R. Schafranek, S. P. Harvey and T. O. Mason, *Thin Solid Films*, 2009, **518**, 1197.
16 T. C. Chiang and F. J. Himpsel, in *Landolt-Börnstein – Group III Condensed Matter*, ed. A. Goldmann and E.-E. Koch, Springer-Verlag, Berlin/Heidelberg, 1989, pp. 15–20.
17 S. Tanuma, C. J. Powell and D. R. Penn, *Surf. Interface Anal.*, 1994, **21**, 165.
18 J. L. Lyons, A. Janotti and C. G. Van de Walle, *Phys. Rev. B: Condens. Matter Mater. Phys.*, 2009, **80**, 205113.
19 J. J. Yeh and I. Lindau, *At. Data Nucl. Data Tables*, 1985, **32**, 1.
20 M. B. Trzhaskovskaya, V. I. Nefdov and V. G. Yarzhemsky, *At. Data Nucl. Data Tables*, 2001, **77**, 97.
21 F. J. Himpsel, F. R. McFeely, A. Taleb-Ibrahimi, J. A. Yarmoff and G. Hollinger, *Phys. Rev. B: Condens. Matter Mater. Phys.*, 1988, **38**, 6084.
22 C. D. Wagner, D. E. Passoja, H. F. Hillery, T. G. Kinisky, H. A. Six, W. T. Jansen and J. A. Taylor, *J. Vac. Sci. Technol.*, 1982, **21**, 933.
23 U. Meier and C. Pettenkofer, *Appl. Surf. Sci.*, 2005, **252**, 1139.
24 X. Xu, C. Guo, Z. Qi, H. Liu, J. Xu, C. Shi, C. Chong, W. Huang, Y. Zhou and C. Xu, *Chem. Phys. Lett.*, 2002, **364**, 57.
25 X. Xu, P. Wang, Z. Qi, H. Ming, J. Xu, H. Liu, C. Shi, G. Lu and W. Ge, *J. Phys.: Condens. Matter*, 2003, **15**, L607.
26 L. S. Dake, D. R. Baer and J. M. Zachara, *Surf. Interface Anal.*, 1989, **14**, 71.
27 K. J. Hubbard and D. G. Schlom, *J. Mater. Sci.*, 1996, **11**, 2757.
28 H. Amekura and N. Kishimoto, in *Toward Functional Nanomaterials*, ed. Z. M. Wang, Springer, US, 2009, pp. 1–75.
29 G. T. Faust, *Am. Mineral.*, 1951, **36**, 795.
30 P. Roura, J. Farjas, C. Rath, J. Serra-Miralles, E. Bertran and P. Roca i Cabarrocas, *Phys. Rev. B: Condens. Matter Mater. Phys.*, 2006, **73**, 085203.
31 A. de Calheiros Velozo, G. Lavareda, C. Nunes de Carvalho and A. Amaral, *Thin Solid Films*, 2013, **543**, 48.
32 A. Reisman, M. Berkenblit, R. Ghez and S. A. Chan, *J. Electron. Mater.*, 1972, **1**, 395.
33 Y. J. Chabal, *Fundamental Aspects of Silicon Oxidation*, Springer, 2001.
34 J. C. Mikkelsen Jr, *Appl. Phys. Lett.*, 1981, **39**, 903.
35 P. Taylor and D. G. Owen, *Polyhedron*, 1984, **3**, 151.
36 F. Iacona, V. Raineri, F. L. Via, V. Privitera, A. Gasparotto and E. Rimini, *J. Electrochem. Soc.*, 2000, **147**, 2762.

37 T. Pangilinan-Ferolin, R. M. Vequizo, Proceedings of the IETEC'13 Conference, Ho Chi Minh City, Vietnam, 2013.
38 H. F. W. Taylor, *Am. Mineral.*, 1962, **47**, 932.
39 A. E. Standage and M. S. Gani, *J. Am. Ceram. Soc.*, 1967, **50**, 101.
40 H. Bracht and N. A. Stolwijk, in *Landolt-Börnstein – Group III Condensed Matter Volume 33A – Diffusion in Semiconductors*, ed. D. L. Beke, Springer-Verlag, Berlin/Heidelberg, 1998, pp. 12–134.
41 C. S. Fuller and F. J. Morin, *Phys. Rev.*, 1957, **105**, 379.